Molybdenum Nanowires by Electrodeposition

Michael P. Zach, Kwok H. Ng, Reginald M. Penner*

Metallic molybdenum (Mo°) wires with diameters ranging from 15 nanometers to 1.0 micrometers and lengths of up to 500 micrometers (0.5 millimeters) were prepared in a two-step procedure. Molybdenum oxide wires were electrodeposited selectively at step edges and then reduced in hydrogen gas at 500°C to yield Mo°. The hemicylindrical wires prepared by this technique were self-uniform, and the wires prepared in a particular electrodeposition (in batches of 10^5 to 10^7) were narrowly distributed in diameter. Wires were obtained size selectively because the mean wire diameter was directly proportional to the square root of the electrolysis time. The metal nanowires could be embedded in a polystyrene film and lifted off the graphite electrode surface. The conductivity and mechanical resiliency of individual embedded wires were similar to those of bulk molybdenum.

One motivation for synthesizing nanowires is their potential use as interconnects in future generations of nanometer-scale electronics. There are few methods for preparing nanowires that are long, uniform in diameter, free-standing, and metallic. Two of the most successful approaches are template synthesis and step-edge decoration. The template synthesis of metal nanowires, pioneered by Martin (*1*), Moskovits (*2*), and Searson (*3*), involves the deposition of metal into the cylindrical pores of an inert, nonconductive host material (such as porous Al_2O_3 films). Step-edge decoration, pioneered by Himpsel (*4, 5*), Kern (*6*), Behm (*7*), and others (*8*), involves the selective deposition of a metal or other material (such as CaF_2) at atomic step edges on a single crystal surface. Step-edge decoration can be controlled to yield continuous "wires" of varied width and interwire spacing (*5*). In the case of metal wires, however, the wire thickness in the direction perpendicular to the surface is just one or at most two atomic layers. These ultrathin metallic ribbons cannot be removed from the surfaces on which they are deposited.

We used the step-decoration method to prepare three-dimensional molybdenum (Mo°) nanowires that range from 15 nm to 1.0 μm in diameter and are removable from the graphite surfaces on which they were synthesized. Our method is summarized in Fig. 1. In the first step of the synthesis, "precursor" nanowires were selectively electrodeposited at step edges on a graphite surface from an alkaline solution of MoO_4^{2-}. As-deposited wires were composed of molybdenum oxides (MoO_x) with diameters from 20 nm to 1.3 μm. These nanostructures were brittle and nonconductive, but highly uniform in diameter. MoO_x wires were then reduced in H_2 at 500°C to produce metallic Mo° nanowires that retained the dimensional uniformity and hemicylindrical shape of the parent composite wires but were smaller in diameter (by 30 to 35%), mechanically resilient, and electronically conductive. After reduction, metallic nanowires that were up to hundreds of micrometers in length were embedded in a polystyrene film and lifted off the graphite surface. In the insulating polymer matrix, the current-voltage (*I-V*) properties of individual wires were measured.

Precursor nanowires composed of MoO_x were obtained by electrodeposition onto freshly cleaved graphite surfaces from dilute, alkaline (pH = 8.5) MoO_4^{2-} solutions. A typical cyclic voltammogram for MoO_4^{2-} at graphite is shown in Fig. 2A (*12*). At deposition potentials, in the range from −0.7 to −0.9 V versus a saturated calomel electrode (SCE) (corresponding to the shaded region shown in the inset to Fig. 2A), electrodeposition occurred with a high degree of selec-

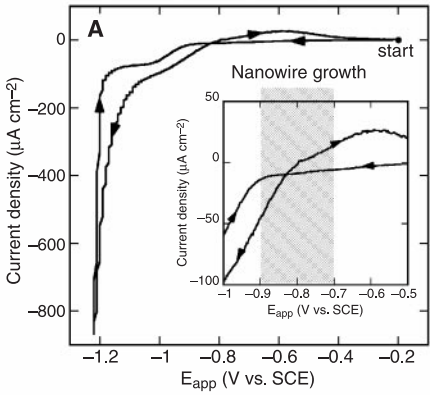

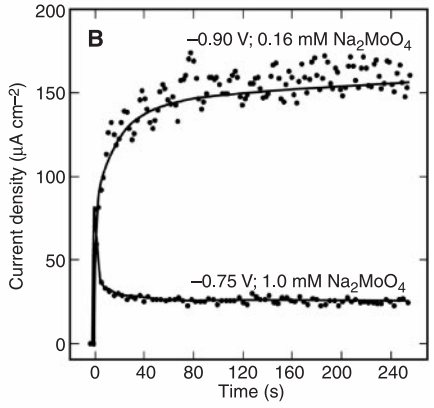

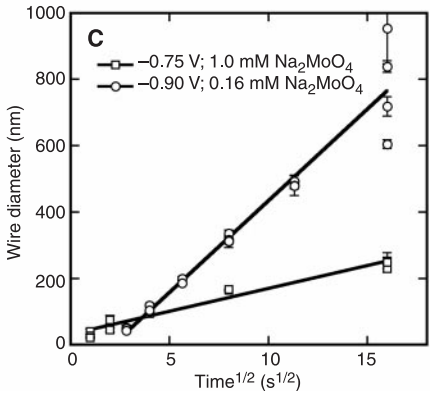

Fig. 2. (**A**) Cyclic voltammogram at 2 mV s^{-1} for a graphite electrode in aqueous 1.0 mM MoO_4^{2-}, 1.0 M NaCl, and 1.0 M NH_4Cl (pH = 8.5). The potential range (relative to an SCE) within which nanowire growth occurs selectively at step edges is indicated in the inset. E_{app}, applied potential (−0.7 to −0.9 V versus SCE). (**B**) Deposition current versus time traces for two depositions conducted with different plating potentials (−0.75 and −0.90 V versus SCE) and MoO_4^{2-} concentrations (1.0 and 0.16 mM) as indicated. (**C**) Diameter of Mo°/MoO_x composite nanowires versus the square root of the deposition time for two series of depositions as indicated. Error bars indicate ±1σ diameter.

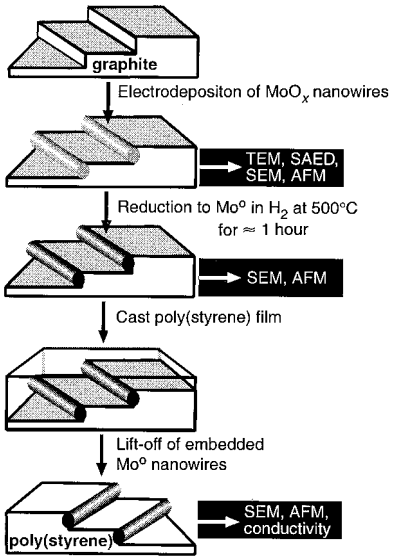

Fig. 1. Summary of the step-decoration method used to prepare three-dimensional Mo° nanowires. TEM, transmission electron microscopy; SAED, selected area electron diffraction; SEM, scanning electron microscopy; AFM, atomic force microscopy.

Institute for Surface and Interface Science, Department of Chemistry, University of California, Irvine, Irvine, CA 92679–2025, USA.

*To whom correspondence should be addressed. E-mail: rmpenner@uci.edu

tivity at step edges. The application of a plating potential more negative than –1.0 V caused particle growth at terraces on the surface to compete with growth at step edges, and with a growth potential of –2.0 V, particle growth (coincident with H_2 evolution) was observed to the exclusion of step-edge decoration [as previously described for nickel (*9*)].

As shown in Fig. 2B, the current associated with nanowire growth at –0.7 to –0.9 V became nearly invariant within 40 s. This rate invariance is consistent with a convection-limited growth process. Under these conditions, the rate law for the growth of a hemicylindrical solid becomes (*10*)

$$r(t) = (2i_{dep}t_{dep}M/\pi nF\rho l)^{1/2} \quad (1)$$

where $r(t)$ is the radius of the hemicylindrical nanowire, i_{dep} is the deposition current, t_{dep} is the deposition time, M is the atomic weight of the deposited metal, n is the number of electrons transferred per metal atom, F is the Faraday constant (96,485 C eq^{-1}), ρ is its density, and l is the total length of the nanowire (or nanowires) on the electrode surface.

As shown in Fig. 2C, the $r(t)$ versus $t^{1/2}$ linearity predicted by Eq. 1 was observed experimentally for nanowires ranging in diameter from 20 nm to 0.9 μm. This linearity has two important consequences. First, it implies that nanowires of any diameter within this range may be prepared by using specified conditions of i_{dep} and t_{dep}, parameters over which we have experimental control. Second, because dr/dt (evaluated from Eq. 1) is proportional to $t^{-1/2}$, the growth rate of small-diameter nanowires (or the relatively small sections of a single nanowire) is greater than that of large-diameter nanowires (or the large sections of an individual nanowire). This proportionality for dr/dt, as established for colloids (*11*), makes possible the growth of highly dimensionally uniform structures—in this case, populations of nanowires that are narrowly dispersed with respect to the wire diameter.

Low-magnification scanning electron microscopy (SEM) images of MoO_x nanowires after electrodeposition show that long, dimensionally uniform nanowires were obtained in large numbers (Fig. 3A). Indeed, nanowires 500 μm in length were routinely obtainable over the entire diameter range from 20 nm to 1.0 μm. Figure 3, B through E, shows two pairs of SEM images that were acquired from the same surface at two magnifications. In Fig. 3C, the smallest nanowires that could be observed by SEM are shown. These structures, which were prepared by using t_{dep} = 1.0 s, had an average diameter of 15 nm; these nanowires were too small to be seen in the lower magnification SEM image of Fig. 3B. After gas-phase reduction, Mo^o nanowires with a diameter of ≈11 nm were obtained. The SEM images in Fig. 3, D and E, show MoO_x nanowires with a diameter of 130 nm prepared with a t_{dep} value of 16.0 s.

All of the nanowires shown in the SEM images of Fig. 3 have diameters that are many times the height of the step edge responsible for nucleating the growth of the wire (typical height, 0.3 to 2 nm). Two factors contribute to this "amplification" of the step edge. First, at the low deposition potentials used, all incipient nucleation sites are confined to step edges on the surface, which helps prevent the "spread" of a nanowire onto terraces during growth. The second factor is the inherent hemicylindrical symmetry of diffusional transport to metal nuclei arrayed along a linear step. These two factors operate in concert and permit the growth of hemicylindrical wires with virtually any diameter from step edges having molecular dimensions.

Energy-dispersive x-ray spectra for as-deposited and reduced nanowires (Fig. 4A) suggest that treatment of MoO_x nanowires with H_2 at 500°C causes their reduction to Mo^o. Specifically, the signal for oxygen in the spectra of as-deposited nanowires disappears upon reduction. Selected area electron diffraction analysis is also consistent with this conclusion. As-deposited nanowires did not reproducibly yield a diffraction pattern (Fig. 4B, top); however, diffraction was observed for reduced nanowires (Fig. 4B, bottom), and the strongest lines in these patterns were assigned to body-centered cubic molybdenum metal (*13*). Weaker diffraction lines for MoO_2 were also observed in these patterns, consistent with the formation of a surface oxide after exposure to air. Finally, the diameter of reduced nanowires contracted by 30 to 35% upon reduction. This contraction of the wire diameter is caused by the smaller molar volume of Mo^o (9.4 cm^3 mol^{-1}), as compared with MoO_x (30.7 cm^3 mol^{-1} for x = 3; 19.8 cm^3 mol^{-1} for x = 2), and can therefore be used to calculate the composition of the as-deposited wires if it can be assumed that these wires consist of a mixture of MoO_2 and MoO_3 and that gas-phase reduction produces nanowires composed of pure Mo^o metal. This calculation suggests that as-deposited MoO_x nanowires are essentially pure MoO_2 (for which the contraction in radius is 31%).

Metallic nanowires can be lifted off the graphite surface by first casting a thin polystyrene film onto the graphite surface. We then allow this film to air-dry, after which we can peel this film with the embedded nanowires off the graphite surface (Fig. 1). The

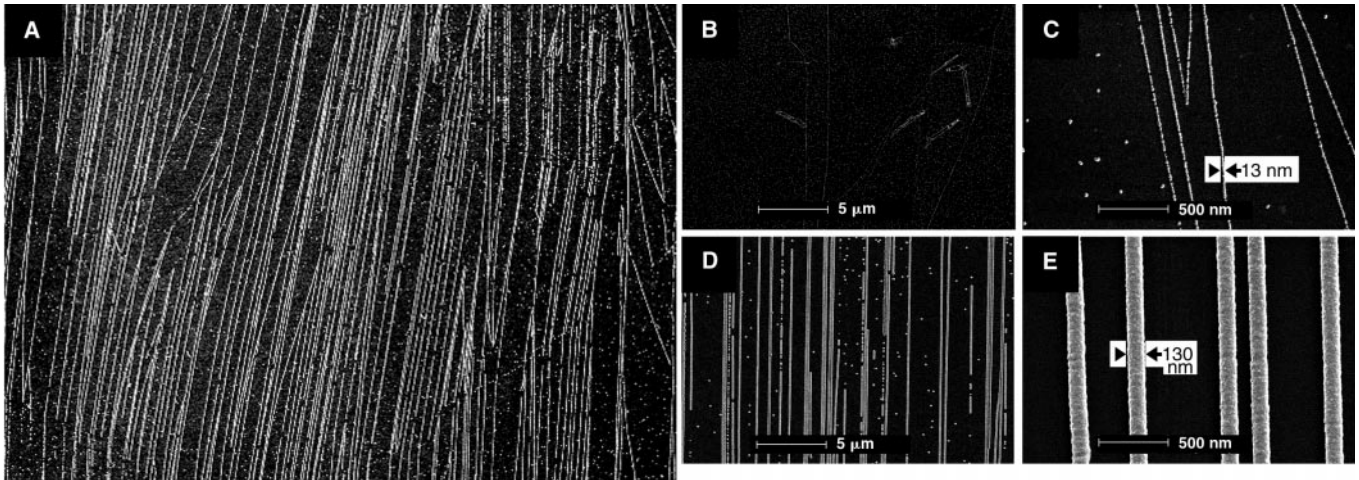

Fig. 3. SEM images of graphite surfaces following the electrodeposition of MoO_x nanowires at –0.75 V versus SCE from a plating solution containing 1.0 mM MoO_4^{2-}. (**A**) Low-magnification SEM image showing the linearity, number density, and uniformity of electrodeposited nanowires. (**B** and **C**) t_{dep} = 1.0 s. (**D** and **E**) t_{dep} = 16.0 s.

surface of one such polystyrene film, together with embedded 200-nm-diameter nanowires, is shown in the SEM images of Fig. 4, C and D. Greater than 80% of the deposited and reduced nanowires could be removed from the graphite surface intact. Embedded nanowires, which were accessible from one side of the insulating polymer film, were ideally disposed for *I-V* measurements, which were carried out by mechanically contacting individual nanowires (down to 300 nm in diameter) with the tip of a gold-coated, 200-nm-diameter glass probe. A second contact to each nanowire was provided by a silver-painted stripe on the polymer surface.

An *I-V* trace for a 380-nm-diameter wire (Fig. 4E) was linear and had a slope that was inversely proportional to the length of the wire isolated in the measurement. These characteristics of ohmic conduction were seen for all of the reduced nanowires investigated for this study. As-deposited nanowires (removed from the graphite surface by using the same embedding procedure) exhibited no measurable conductivity. For reduced nanowires, the measured value of the resistivity increased as a function of the air exposure time after reduction. In Fig. 4F, for example, the resistivity of a 380-nm-diameter wire just 2 hours after reduction (5.5×10^{-5} ohm·cm) was a factor of ~10 greater than that expected for a nanowire of the same diameter composed of bulk Mo° metal (5.34×10^{-6} ohm·cm). In contrast, a 480-nm nanowire that was allowed to age in air for 48 hours after reduction exhibited a resistivity of more than 300 times that expected for bulk Mo°. We conclude that the surface of a reduced Mo° nanowire is converted by air oxidation to nonconductive MoO_x on the time scale of a few hours.

The mechanical properties of nanowires larger than 300 nm in diameter were also observable after transfer to the polystyrene film. Individual embedded nanowires selected for observation were anchored at one end with silver paint (as seen on the right-hand side of the optical micrographs in Fig. 5 for a 300-nm-diameter Mo° wire). A suspended nanowire was then obtained by dislodging the other end of the nanowire from the polymer film with the same 200-nm glass probe used for conductivity measurements (Fig. 5A). The response of this suspended nanowire to the application of a lateral force from the probe provided a qualitative indication of its flexibility and resiliency. In Fig. 5B, the suspended nanowire was first bent by 90°, released (Fig. 5C), and then bent by 90° again (Fig. 5D). This degree of resiliency was a characteristic of reduced Mo° nanowires, and

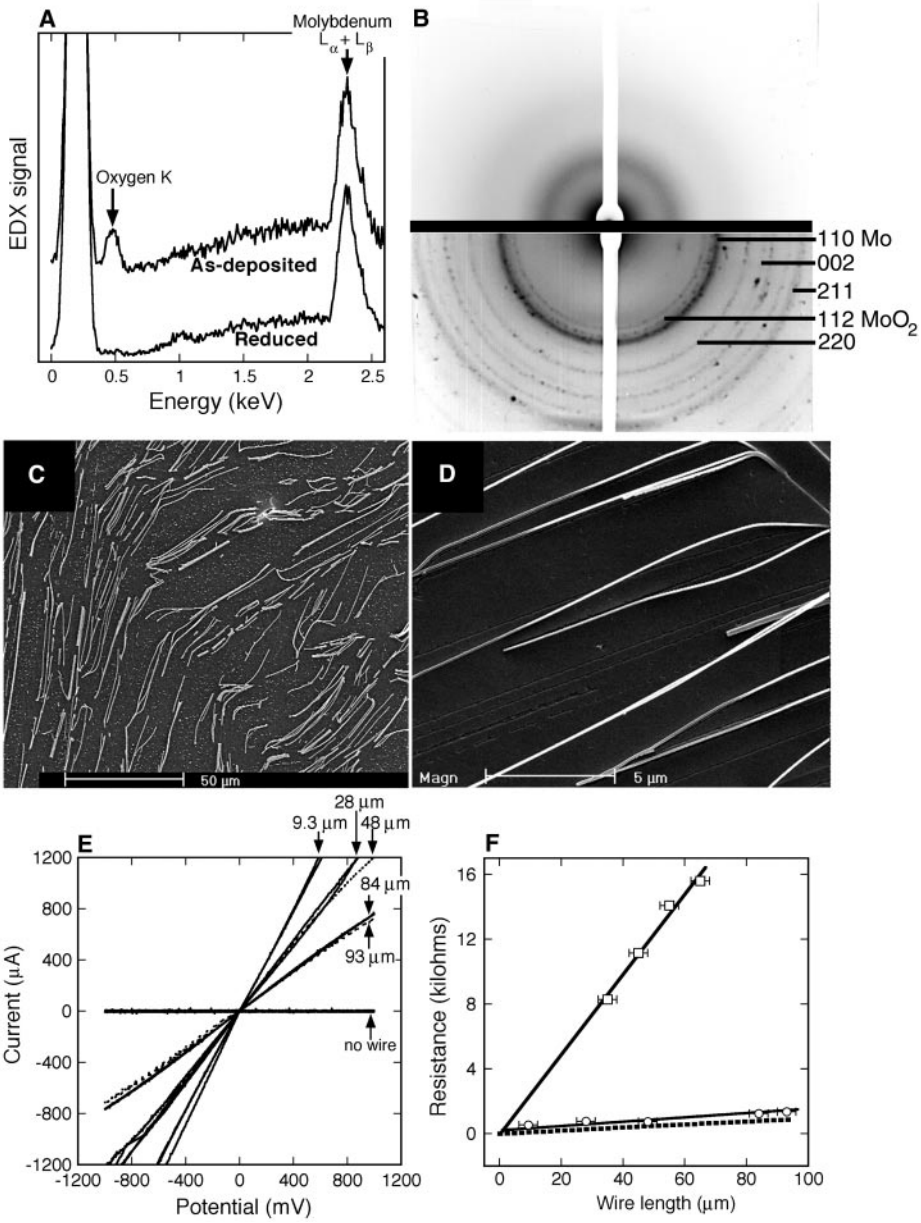

Fig. 4. (**A**) Energy dispersive x-ray (EDX) elemental analysis traces for as-deposited and reduced nanowires. L_α and L_β are the transitions responsible for these x-ray fluorescence lines. (**B**) Selected area electron diffraction patterns for as-deposited (top) and reduced (bottom) nanowires. The diffraction assignments shown in (B) correspond to body-centered cubic molybdenum metal and monoclinic MoO_2. (**C** and **D**) SEM images of a polystyrene film in which reduced molybdenum nanowires are embedded. (**E**) *I-V* traces for a 380-nm-diameter Mo° nanowire. Five traces, acquired by electrically isolating various lengths of this wire (as indicated) are shown. (**F**) Plot of the measured resistance at 0.0 V as a function of the nanowire length for two nanowires with diameters of 450 nm (squares, 48 hours after reduction) and 380 nm (circles, 2 hours after reduction). The resistivities for these wires (derived from the slopes of these plots) are $\rho = 2.0 \times 10^{-3}$ ohm·cm (squares) and $\rho = 5.5 \times 10^{-5}$ ohm·cm (circles). Also shown (dashed line) is the predicted resistance versus length plot for a 380-nm-diameter nanowire composed of pure Mo° ($\rho = 5.34 \times 10^{-6}$ ohm·cm). Error bars indicate $\pm 1\sigma$ length.

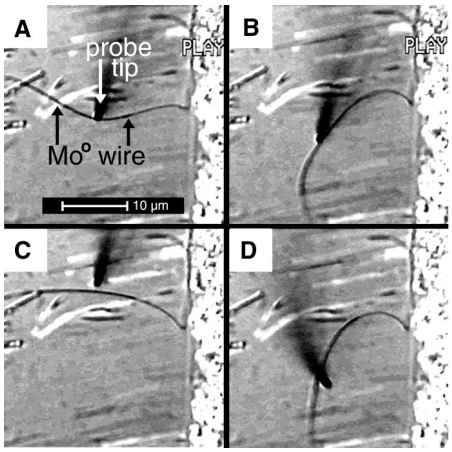

Fig. 5. (**A** through **D**) Optical micrographs showing the bending of a suspended Mo° nanowire with a glass probe tip.

it provides further evidence of the conversion of these nanostructures to Mo°. In contrast, as-deposited MoO_x composite nanowires were brittle and were subject to breaking when flexed by as little as 5°.

We conducted a survey of other metals and discovered that noble metals, including silver, platinum, and copper, do not nucleate with a sufficiently high linear density along step edges on graphite to form continuous nanowires, but instead form disconnected linear arrays of micrometer-scale metal particles. These three metals all exhibited facile electrodeposition kinetics at graphite surfaces. In contrast, several base metals, all of which exhibit slow heterogeneous electron transfer kinetics for deposition, behaved similarly to molybdenum. For example, we obtained nanowires of cadmium and nickel-molybdenum alloy by using deposition conditions analogous to those used in this study.

References and Notes

1. C. A. Foss, M. J. Tierney, C. R. Martin, *J. Phys. Chem.* **96**, 9001 (1992); C. R. Martin *et al.*, *Adv. Mater.* **11**, 1021 (1999); S. A. Sapp, D. T. Mitchell, C. R. Martin, *Chem. Mater.* **11**, 1183 (1999).
2. C. K. Preston, M. Moskovits, *J. Phys. Chem.* **97**, 8495 (1993); D. Routkevitch, T. Bigioni, M. Moskovits, J. M. Xu, *J. Phys. Chem.* **100**, 14037 (1996); D. N. Davydov *et al.*, *Phys. Rev. B* **57**, 13550 (1998).
3. L. Sun, P. C. Searson, C. L. Chien, *Phys. Rev. B* **61**, R6463 (2000); T. M. Whitney, J. S. Jiang, P. C. Searson, C. L. Chien, *Science* **261**, 1316 (1993); L. Sun, P. C. Searson, C. L. Chien, *Appl. Phys. Lett.* **74**, 2803 (1999).
4. F. J. Himpsel *et al.*, *MRS Bull.* **24**, 20 (1999); T. Jung, R. Schlittler, J. K. Gimzewski, F. J. Himpsel, *Appl. Phys. A* **61**, 467 (1995).
5. D. Y. Petrovykh, F. J. Himpsel, T. Jung, *Surf. Sci.* **407**, 189 (1998).
6. M. Blanc, K. Kuhnke, V. Marsico, K. Kern, *Surf. Sci.* **414**, L964 (1998); P. Gambardella, M. Blanc, H. Brune, K. Kuhnke, K. Kern, *Phys. Rev. B* **61**, 2254 (2000).
7. R. J. Nichols, D. M. Kolb, R. J. Behm, *J. Electroanal. Chem.* **313**, 109 (1991); S. Morin, A. Lachenwitzer, O. M. Magnussen, R. J. Behm, *Phys. Rev. Lett.* **83**, 5066 (1999).
8. E. A. Abd El Meguid, P. Berenz, H. Baltruschat, *J. Electroanal. Chem.* **467**, 50 (1999); J. Dekoster *et al.*, *Appl. Phys. Lett.* **75**, 938 (1999).
9. M. P. Zach, R. M. Penner, *Adv. Mater.* **12**, 878 (2000).
10. Eq. 1 is readily derived from the expression for the deposition charge associated with the formation of a hemicylindrical solid, $Q_{dep} = (\pi r^2 n F \rho l/2M)$. For deposition with a constant current i_{dep}, $Q_{dep} = i_{dep} t_{dep}$. Eq. 1 is then obtained by solving for $r(t)$ in this equation.
11. M. T. Reetz, W. Helbig, *J. Am. Chem. Soc.* **116**, 7401 (1994); V. K. LaMer, R. H. Dinegar, *J. Am. Chem. Soc.* **72**, 4847 (1950); T. Sugimoto, *Adv. Colloid Interface Sci.* **28**, 65 (1987).
12. A more extensive version of Fig. 3 is available at www.sciencemag.org/cgi/content/full/290/5499/2120/DC1.
13. The lattice parameter for body-centered cubic molybdenum metal is 3.1472 Å. Lattice parameters for monoclinic MoO_2 are $a = 5.6096$ Å, $b = 4.857$ Å, and $c = 5.6259$ Å, and $\beta = 120.912$.

14. This work was funded by the NSF (grant DMR-9876479) and the Petroleum Research Fund of the American Chemical Society (grant 33751-AC5). We also gratefully acknowledge the financial support of the Camille and Henry Dreyfus Foundation. Finally, donations of graphite by A. Moore of Advanced Ceramics are gratefully acknowledged.

11 August 2000; accepted 13 October 2000

High-Resolution Inkjet Printing of All-Polymer Transistor Circuits

H. Sirringhaus,[1]* T. Kawase,[1]† R. H. Friend,[1]* T. Shimoda,[2] M. Inbasekaran,[3] W. Wu,[3] E. P. Woo[3]

Direct printing of functional electronic materials may provide a new route to low-cost fabrication of integrated circuits. However, to be useful it must allow continuous manufacturing of all circuit components by successive solution deposition and printing steps in the same environment. We demonstrate direct inkjet printing of complete transistor circuits, including via-hole interconnections based on solution-processed polymer conductors, insulators, and self-organizing semiconductors. We show that the use of substrate surface energy patterning to direct the flow of water-based conducting polymer inkjet droplets enables high-resolution definition of practical channel lengths of 5 micrometers. High mobilities of 0.02 square centimeters per volt second and on-off current switching ratios of 10^5 were achieved.

Semiconducting organic molecules (*1*) and polymers (*2*) can be self-assembled from solution into ordered structures with charge carrier mobilities close to that of inorganic thin-film silicon. They may form the basis of a new thin-film electronic technology, in which integrated transistor circuits are manufactured by cheap solution processing and direct printing rather than vacuum deposition and photolithographic patterning (*3*–*6*). However, this requires the development of printing techniques that provide accurate definition of all components of an integrated circuit but do not compromise the ability of the organic molecules to self-assemble. Inkjet printing (IJP) has emerged as an attractive patterning technique for conjugated polymers in light-emitting diodes (*7, 8*) and full-color high-resolution displays (*9*). The technique has not been applied to organic transistors yet, because its resolution is limited to 20 to 50 μm by statistical variations of the flight direction of droplets and their spreading on the substrate. This is not sufficient for defining source-drain electrodes of practical thin-film transistors (TFTs) without accidental electrical shorts. Channel lengths of $L = 5$ to 10 μm are required to achieve adequate drive current and switching speed.

Our approach for overcoming this problem is to confine the spreading of water-based conducting polymer ink droplets on a hydrophilic substrate with a pattern of narrow, repelling, hydrophobic surface regions that define the critical device dimensions (Fig. 1A). This surface free energy pattern on the Corning 7059 glass substrate is fabricated before TFT deposition by photolithography and O_2 plasma etching of a 500 Å polyimide film (*9*). After etching through the polyimide, the O_2 plasma renders the source-drain regions on the bare glass hydrophilic, whereas the polyimide line defining the TFT channel is protected by photoresist and remains hydrophobic. The contact angle of water on hydrophilic glass and hydrophobic polyimide is 20° to 25° and 70° to 80°, respectively. For the source-drain and gate electrodes we use a water-based ink of the conducting polymer poly(3,4-ethylenedioxythiophene) doped with polystyrene sulfonic acid (PEDOT/PSS, Baytron P from Bayer, Krefeld, Germany). Our home-built, piezoelectric inkjet printer is equipped with an optical imaging system that allows coarse alignment (± 5 μm) of the inkjet nozzles with respect to the polyimide substrate pattern. A line of PEDOT droplets is deposited into the hydrophilic regions at a distance d from the polyimide line that is sufficiently small for the spreading droplets to reach the repelling line. The lateral distance between successive droplets (10 to 20 μm) is smaller than the radius of sessile droplets (≈80 μm). Each droplet dries partially before the next droplet is deposited.

Atomic force microscopy (AFM) (Fig. 1B) shows that the inkjet-deposited PEDOT electrodes extend precisely up to the repelling polyimide line, whereas the second, unconfined boundary of the PEDOT line exhibits a typical roughness of ±10 μm (Fig. 1D). No PEDOT deposition occurs on top of the poly-

[1]Cavendish Laboratory, University of Cambridge, Madingley Road, Cambridge CB3 OHE, UK. [2]Base Technology Research Center, Seiko-Epson Corporation, 3-5-3 Owa, Suwa-Shi, Nagano-Ken 392, Japan. [3]The Dow Chemical Company, Midland, MI 48674, USA.

*To whom correspondence should be addressed. E-mail: hs220@phy.cam.ac.uk

†Also at Epson Cambridge Laboratory, 8c King's Parade, Cambridge CB2 1SJ, UK.